NANO LETTERS

Letter

Identifying Individual Single-Walled and Double-Walled Carbon Nanotubes by Atomic Force Microscopy

Tristan DeBorde, J. Caleb Joiner, Matthew R. Leyden, and Ethan D. Minot

Nano Lett., **2008**, 8 (11), 3568-3571• DOI: 10.1021/nl801106p • Publication Date (Web): 24 September 2008

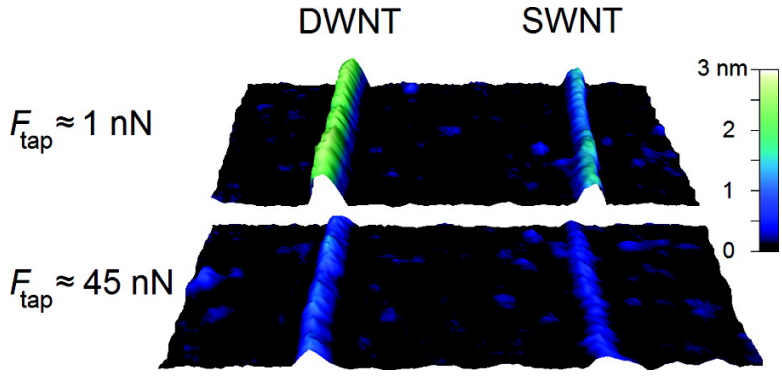

More About This Article

Additional resources and features associated with this article are available within the HTML version:

- Supporting Information
- Access to high resolution figures
- Links to articles and content related to this article
- Copyright permission to reproduce figures and/or text from this article

View the Full Text HTML

NANO LETTERS

2008
Vol. 8, No. 11
3568-3571

Identifying Individual Single-Walled and Double-Walled Carbon Nanotubes by Atomic Force Microscopy

Tristan DeBorde, J. Caleb Joiner, Matthew R. Leyden, and Ethan D. Minot*

Department of Physics, Oregon State University, Corvallis, Oregon 97330

Received April 17, 2008; Revised Manuscript Received August 15, 2008

ABSTRACT

We show that the number of concentric graphene cylinders forming a carbon nanotube can be found by squeezing the tube between an atomic force microscope tip and a silicon substrate. The compressed height of a single-walled nanotube (double-walled nanotube) is approximately two (four) times the interlayer spacing of graphite. Measured compression forces are consistent with the predicted bending modulus of graphene and provide a mechanical signature for identifying individual single-walled and double-walled nanotubes.

The electronic and mechanical properties of carbon nanotubes (CNTs) depend on the number of concentric cylinders forming the CNT. The additional shells of a multiwalled nanotube, or neighboring tubes in a nanotube bundle, create parallel conduction paths and alter the electronic environment. Similarly, the radial compressibility of CNTs is affected by additional shells or bundling. Techniques to determine shell number or bundling, such as transmission electron microscopy, are often not compatible with experimental geometries for electrical and mechanical measurements. In such cases, researchers must rely on indirect evidence, such as the uncompressed height of a nanotube, to guess the exact shell structure.

Many authors have investigated stress−strain relationships of CNTs in the axial and radial directions;[1−6] however, these mechanical measurements have not demonstrated the resolution required to distinguish between single-walled nanotubes (SWNTs), double-walled nanotubes (DWNTs), and nanotube bundles. In this work we show that individual SWNTs and DWNTs have distinct mechanical signatures that are readily measured by atomic force microscopy (AFM). We have compared our measurements to a simple mechanical model that is based on theoretical predictions of the bending modulus of graphene.[7]

Carbon nanotubes were prepared on silicon substrates by either drop-casting commercially available CNTs (a mixture of DWNTs and SWNTs from Carbon Nanotechnologies Inc.) or by the chemical vapor deposition growth method.[8] Silicon AFM tips (Budget Sensors) with nominal spring constant $k = 40$ N/m and quality factor $Q \approx 400$ were characterized using the thermal amplitude method[9] and tip radius was found using $R_{tip} = w^2/8h$ where w and h are the apparent width and height of a nanotube imaged by AFM. For ac-mode imaging the cantilever was driven close to resonance; the phase difference ϕ between cantilever motion and the driving piezo was $90 \pm 5°$ before engaging with the sample.

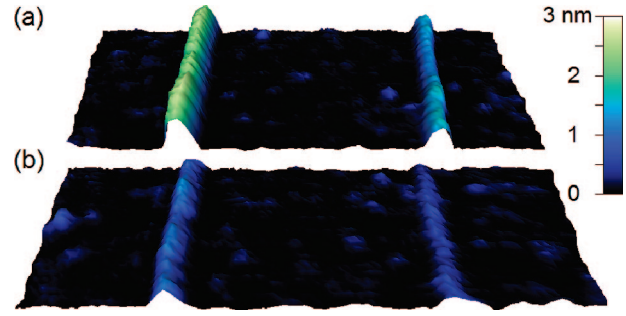

Figure 1. (a) Atomic force microscope image of two CVD grown nanotubes on a silicon substrate when energy transfer between tip and sample is small: $A_{free} = 11.5$ nm, $A_{setpoint} = 10.6$ nm, $\phi = 116°$ ($E_{tap} \sim 1$ eV). (b) Image of the same nanotubes when $A_{free} = 86$ nm, $A_{setpoint} = 43$ nm, $\phi = 43°$. The same height scale applies to both panels a and b. $R_{tip} = 29$ nm and $k = 20.3$ N/m.

Figure 1a shows an ac-mode AFM image (Asylum Research MFP-3D) of two CNTs with heights $h = 2.4$ and 1.5 nm. Compression of the two nanotubes during this image was minimized by driving the cantilever with a small free-air amplitude $A_{free} = 11.5$ nm and imaging with a correspondingly small amplitude set-point $A_{setpoint} = 10.5$ nm. The phase ϕ was monitored during imaging and remained $>90°$ (attractive mode imaging[11]). Figure 1b shows the same nanotubes imaged with $A_{free} = 86$ nm, $A_{setpoint} = 43$ nm, and $\phi < 90°$. The measured nanotube heights decrease to $h = 1.05$ and 0.55 nm, respectively. The reduction in h is

* To whom correspondence should be addressed. E-mail: minote@science.oregonstate.edu.

10.1021/nl801106p CCC: $40.75
Published on Web 09/24/2008

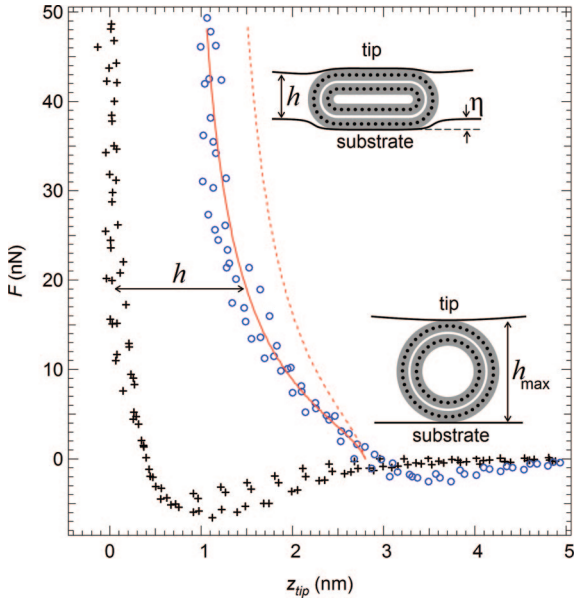

Figure 2. Force−distance measurements of the larger CNT in Figure 1 and nearby points on the silicon substrate. Crosses show the AFM tip engaging with the substrate with data from four different trials (two on the left side of the CNT and two on the right side). Circles show the tip engaging with the DWNT with data from three different trials. Inset drawings show cross sections of the CNT during compression. Carbon ions in the CNT are represented by black dots. Grey bands depict the thickness of graphene, t, due to the electron cloud. For all measurements R_{tip} = 29 nm, dz_{base}/dt = 50 nm/s, data acquisition rate = 200 Hz and data is filtered with a lowpass cutoff of 100 Hz. The dashed red line shows results of the graphene-bending model without considering additional substrate indentation. The solid red line shows results of the model when additional substrate indentation is included.

reversible, and we see no evidence of mechanical damage to the nanotubes, the tip, or the substrate during our experiments.

The "gentle" imaging parameters used for Figure 1a are suitable for measuring the uncompressed height of a nanotube h_{max}.[10] Although the hammering force of the AFM tip on the sample is not a directly measured parameter in ac-mode AFM imaging, it is known that energy transfer from the tip to the sample is small when A_{free} is small and $\phi > 90°$. In Figure 1a, for example, E_{tap} the energy transferred from the tip to the sample during each cycle of cantilever motion was approximately 1 eV (energy dissipation calculations are described in Supporting Information). The "aggressive" imaging parameters used for Figure 1b clearly result in higher hammering forces (reduced h). We show below that this force is sufficient to flatten a SWNT or DWNT.

To quantify the compression of the larger nanotube in Figure 1b (h_{max} = 2.4 nm), we measured h as a function of radial compression force F. After acquiring an ac-mode image of the nanotube, the driven oscillation of the cantilever was stopped and the static deflection of the cantilever, Δ_{tip}, was monitored as the base of the cantilever was moved perpendicular to the surface by a distance z_{base}. Figure 2 shows the downward force, $F = k\Delta_{tip}$, acting on the sample as a function of tip position, $z_{tip} = z_{base} + \Delta_{tip}$, when the tip

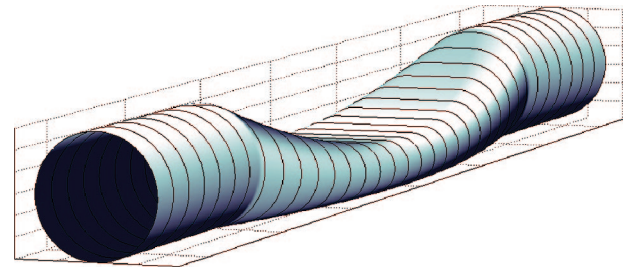

Figure 3. Diagram showing the geometry of a CNT squashed by an AFM tip when $R_{tip} = 10D_{outer}$.

is engaged on either the substrate or the nanotube. To ensure that the tip was centered on the nanotube, a sequence of $F(z_{tip})$ curves were measured on a line of x-y coordinates which bisected the nanotube. Five measurements clearly engaged with the nanotube, and the three well-centered measurements are displayed in Figure 2. There is a time delay of several seconds between each $F(z_{tip})$ measurement. During this delay, thermal drift changes z_{base} by a random distance of the order 1 nm. To account for this drift, curves have been translated on the z_{tip} axis so that substrate and nanotube are separated by h_{max} = 2.4 nm when F = 0. As F is increased from 0 to 50 nN, a 0.45 nm elastic deformation is observed on the substrate and a 1.8 nm elastic deformation is observed on the CNT. At F = 50 nN the substrate and nanotube curves are separated by 1.05 nm.

The minimum height 1.05 nm measured in Figure 1b and Figure 2 is consistent with expectations for a DWNT. The interlayer spacing of uncompressed graphite is 0.34 nm. Under high pressure (near the graphite-diamond transition), the interlayer spacing reaches 0.21 nm.[12] Therefore, if forces are sufficient to flatten the cross-section of a nanotube we naively expect 0.42 nm < h < 0.68 nm for SWNTs (the height of two graphene sheets under compression), and 0.84 nm < h < 1.36 nm for DWNTs. While this simple picture neglects nanoindentation of the substrate and the AFM tip (discussed below), minimum height is a useful way to tentatively assign a nanotube as SWNT or DWNT.

To confirm that the CNT is indeed double-walled we compare $F(h)$ to predictions based on the bending modulus of graphene. First principles modeling predicts that the energy cost per atom associated with bending a single sheet of graphene into a cylinder of diameter D is $U_{atom} = \beta/D^2$, where β varies between 47 and 62 meV/nm^2 depending on details of the calculation.[7] We model the nanotube as two concentric graphene cylinders with $D_{outer} = h_{max} - t$ and $D_{inner} = h_{max} - 3t$ (see Figure 2), where $t \approx 0.34$ nm[13] and β = 55 meV/nm^2. (Note that the diameter of the outer ionic lattice will be slightly smaller than h_{max} due to the electron cloud surrounding the ionic lattice). When the tube is compressed by the AFM tip (R_{tip} = 29 nm), the geometry is similar to a garden hose squashed by a basketball (Figure 3). The radius of curvature of the AFM tip is much larger than D_{outer}, therefore when calculating bending energy the nanotube can be treated as mechanically decoupled rings. As rings evolve from circles to stadiums, bending energy is stored in the curved portion of the stadiums. The more the nanotube is

squeezed, the more rings come into contact with the AFM tip. Using this model, we calculate the stored energy due to bending, $U_{total} = \sum U_{atom}$, and the corresponding compression force $F = |dU_{total}/dz_{tip}|$. The dashed line in Figure 2 shows the results of this fully constrained model.

The discrepancy between measured $F(h)$ and the simple graphene-bending model (dashed line in Figure 2) is likely due to indentation of the AFM tip and the substrate. Figure 2 shows that some indentation occurs when the tip engages with bare silicon. Indentations will be even greater when a CNT is sandwiched between the two silicon surfaces due to the reduced contact area. The depth of the elastic indentation caused by a rigid sphere of radius R pressing on a flat silicon substrate is[14]

$$\eta = \left(\frac{3}{4\sqrt{R}}\frac{(1-\nu_{Si})}{E_{Si}}F\right)^{2/3}$$

where $E_{Si} \approx 140$ GPa and $\nu_{Si} \approx 0.2$ are the Young's modulus and Poisson ratio of silicon. The AFM tip will deform a similar amount leading to a total deformation $2\eta \approx 0.3$ nm at $F = 50$ nN. When the CNT is present in the sandwich, a similar analysis based on effective contact area yields $2\eta \approx 0.6$ nm at $F = 50$ nN (the effective contact area is estimated as a fraction of the flattened nanotube surface in Figure 3). The additional indentation due to the presence of the CNT has the correct magnitude and functional form to explain the discrepancy between measured $F(z_{tip})$ and the simple graphene-bending model. We conclude that our measurements are consistent with predictions for a DWNT pushed by a silicon tip into a silicon substrate.

The effect of additional substrate indentation can be incorporated into the graphene-curvature model in a very simple way. A small increase in D_{outer} and D_{inner} simulates the extra space $\eta(F)$ created when the CNT sinks into the substrate. The solid curve in Figure 2 shows the graphene-curvature model with $D_{outer} = h_{max}$ and $D_{inner} = h_{max} - 2t$, no other parameters have been changed with respect to the dashed line. It appears to be a coincidence that $\eta(F)$ is a similar magnitude to t, leading to this simple relationship between h_{max} and D_{outer} used for modeling.

The close agreement between the mechanical model and radial compression measurements (Figure 2) suggests that force-height data can be used as a signature to distinguish between SWNTs, DWNTs, and nanotube bundles. We tested the model on a possible SWNT (the smaller nanotube in Figure 1) by determining h as a function of tapping force F_{tap}. A series of images were obtained with different A_{free} and $A_{setpoint}$ values. For each image, F_{tap} was determined by measuring the height of the DWNT and comparing to the known force-height relationship of the DWNT (Figure 2). The uniformity of F_{tap} across the image was inferred from energy dissipation maps which showed equal energy dissipation on the substrate and on the centerlines of the two nanotubes (see Supporting Information). Figure 4 shows the resulting $h(F_{tap})$ curve of the smaller nanotube. The nanotube reaches a minimum height of 0.55 nm at 25 nN, and the $h(F_{tap})$ curve is in excellent agreement with the prediction of our mechanical model for a single graphene cylinder of diameter 1.5 nm. We conclude that the nanotube is indeed single-walled.

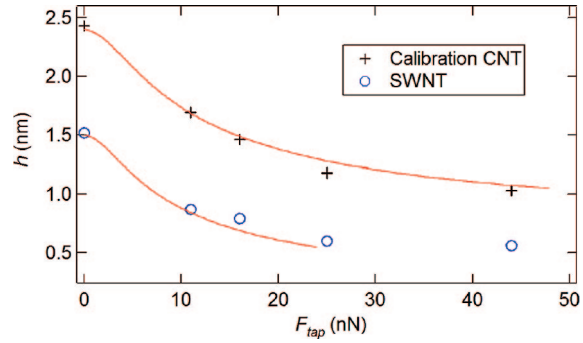

Figure 4. Nanotube height measured by ac-mode AFM at various imaging parameters. The CNT measured in Figure 2 is used to calibrate F_{tap}. Heights were extracted from AFM images by finding the average z coordinate on top of the nanotube (20 pixel average) and subtracting the average height of the substrate (~100 × 100 pixel average). The solid lines are modeled $h(F)$ for a DWNT and a SWNT with $D_{outer} = 2.4$ and 1.5 nm, respectively. The high force region, where graphene cylinders are completely flattened, has not been modeled. Imaging parameters (A_{free} (nm), A_{set} (nm), φ) from smallest to largest F_{tap} are as follows (11.5, 10.6, 116°), (44.7, 39.7, 76°), (57.3, 42.5, 61°), (71.6, 42.5, 49°), and (86.1, 42.5, 43°).

The calibrated F_{tap} imaging technique described above circumvents experimental issues associated with measuring force−distance curves of smaller diameter CNTs (it is very difficult to obtain $F(z_{tip})$ data such as Figure 2 on SWNTs, as evidenced by previous attempts[5,6]). We have used this technique on both silicon and silicon oxide substrates to identify SWNTs and DWNTs (further examples are provided in Supporting Information). In all cases we found close agreement between experimental $h(F_{tap})$ curves and the appropriate SWNT/DWNT mechanical model with $D_{outer} = h_{max}$ and $\beta = 55$ meV/nm^2.

In conclusion, measurements of h as a function of compression force (F or F_{tap}) can be used to identify individual SWNTs and DWNTs. This AFM characterization technique will be useful for future investigation of the mechanical and electrical properties of CNT with known structure. Our measurements of radial compression are consistent with a graphene bending modulus $\beta = 55 \pm 10$ meV/nm^2 and highlight the importance of considering substrate indentation. More accurate determination of β will be possible by detailed modeling of the experiments described here, and future experiments using AFM tips and substrates made from high Young's modulus materials such as diamond.

Acknowledgment. We thank Guenter Schneider and Jason Li for useful discussions.

Supporting Information Available: Scatter plot of $h(F_{tap} \sim 50$ nN) versus h_{max} for all nanotubes with $h_{max} < 1.5$ nm. Map of E_{tap} when imaging nanotubes in Figure 1. $h(F_{tap})$ curve for another DWNT on a silicon substrate. $h(F_{tap})$ curves for a SWNT and a bundle of two SWNTs on thermally grown silicon oxide. Details of the F_{tap} calibration procedure. This material is available free of charge via the Internet at http://pubs.acs.org.

References

(1) Qian, D.; Wagner, G. J.; Ruoff, R. S.; Yu, M. F.; Liu, W. K. *Appl. Mech. Rev.* **2002**, *55* (2), 495–533.

(2) Palaci, I.; Fedrigo, S.; Brune, H.; Klinke, C.; Chen, M.; Riedo, E. *Phys. Rev. Lett.* **2005**, *94* (17), 175502.

(3) Yu, M. F.; Kowalewski, T.; Ruoff, R. S. *Phys. Rev. Lett.* **2000**, *85* (7), 1456–1459.

(4) Shen, W. D.; Jiang, B.; Han, B. S.; Xie, S. S. *Phys. Rev. Lett.* **2000**, *84* (16), 3634–3637.

(5) Fraxedas, J.; Rius, G.; Perez-Murano, F.; Verdaguer, A. *Europhys. Lett.* **2007**, *78*, 16001.

(6) Wang, H. Y. Z. M.; Mao, S. X. *Appl. Phys. Lett.* **2006**, *89*, 211906.

(7) Robertson, D. H.; Brenner, D. W.; Mintmire, J. W. *Phys. Rev. B* **1992**, *45* (21), 12592–12595.

(8) Kong, J.; Soh, H. T.; Cassell, A. M.; Quate, C. F.; Dai, H. J. *Nature* **1998**, *395* (6705), 878–881.

(9) Hutter, J. L.; Bechhoefer, J. *Rev. Sci. Instrum.* **1993**, *64*, 1868–1873.

(10) Postma, H. W. C.; Sellmeijer, A.; C., D. *Adv. Mater.* **2000**, *12*, 1299–1302.

(11) Cleveland, J. P.; Anczykowski, B.; Schmid, A. E.; Elings, V. B. *Appl. Phys. Lett.* **1998**, *72* (20), 2613–2615.

(12) Alder, B. J.; Christian, R. H. *Phys. Rev. Lett.* **1961**, *7* (10), 367–370.

(13) Kiang, C. H.; Endo, M.; Ajayan, P. M.; Dresselhaus, G.; Dresselhaus, M. S. *Phys. Rev. Lett.* **1998**, *81*, 1869–1872.

NL801106P